An Integrated Modeling Approach for Management of Process-Induced Properties in Friction Stir Welding Processes

El-Gizawy A. Sherif [1, 2], Chitti Babu S[2], and Bogis Haitham[1]

[1]Center of Excellence for Industrial Design and Manufacturing Research (CEIDM) Mechanical Engineering, King Abdulaziz University, Jeddah, Saudi Arabia
[2]Industrial and Technological Development Center, Mechanical and Aerospace Engineering, University of Missouri-Columbia Columbia, Missouri 65211, USA

Abstract

Numerical and physical modeling techniques are used to predict process behavior in friction stir welding (FSW) high strength aluminum alloys. The numerical approach uses a non-linear finite element method to characterize thermal and deformation behavior along the welded structure during FSW. Coupled temperature-displacement analysis is applied in order to determine temperature, displacement, and mechanical responses simultaneously. The physical modeling approach uses the response surface methodology (RSM) to evaluate the effects of the process controlling parameters on the properties of the welded joints. The results obtained, offer insights into the effects of the major process parameters in establishing successful FSW joints that satisfy further processing requirements and product service conditions.

Keywords: Friction stir welding; Non-linear finite element analysis; Process-induced properties; Response surface methodology

Introduction

Friction stir welding (FSW) is a solid state welding process where localized deformation at the joint interface establishes the bond between the base metals Figure 1. In this process, a rotating tool generates heat and deformation at the joint interface [1-4]. The interface temperature never exceeds the melting point of the base metals (maximum 90% of melting temperature) [5]. Therefore FSW does not involve liquid phase transformation. This makes the process superior to all other welding processes that result in unfavorable microstructures and properties associated with solidification mechanisms in fusion welding. FSW has many other significant advantages including controlled properties and microstructure, improved material utilization (light weight structures), improved energy utilization (only 2.5% of energy needed for fusion welding), and reduced harmful effects on environment [2-4]. Research in FSW has focused on developing experimental, analytical, and numerical models in order to characterize the different zones in FSW [5-11]. They include the heat affected zone (HAZ), the thermo-mechanically affected zone (TMAZ), and the base metal. The properties of FSW joints are related to the properties and microstructure of different zones in the joint. FSW cycle consists of four stages: plunge stage (the rotating tool is plunged vertically into the joint);dwell stage (tool is held in the plunging position while still rotating); welding stage (rotating tool travel along the joint at constant velocity); and pulling tool out stage (tool is pulled out of the joint leaving behind an exit hole). The parameters that influence the performance of FSW are displayed in Figure 1. They include tool rotational speed, travel speed of the tool, plunge force, plunge depth, and tool design [2-13]. These parameters affect the thermo-mechanical and metallurgical changes established during FSW which in turn are related to the evolved properties, microstructure, and process-induced damage in the course of the welding process.

Research has been carried out to develop the numerical models to simulate friction stir welding. Chao and Qi [14] used a constant heat flux input from tool shoulder/work piece to increase the temperature and trial and error method was used to adjust the heat input. Frigaard, Grong and Midling [15] developed a model for friction stir welding. Heat input was assumed to be the frictional heat and co-efficient of friction and other conditions were adjusted to keep the temperature below the melting point. Zahedul, Khandkar, and Khan [16] modeled the friction stir welding with a moving heat source. The above researches account only for the heat generated by friction between tool shoulder and sheet surface. They did not account for heat generated at the interface between tool pin and sheet materials as well as the heat produced by plastic deformation. Other investigators have attempted to include all components of heat source in their models. Askari used
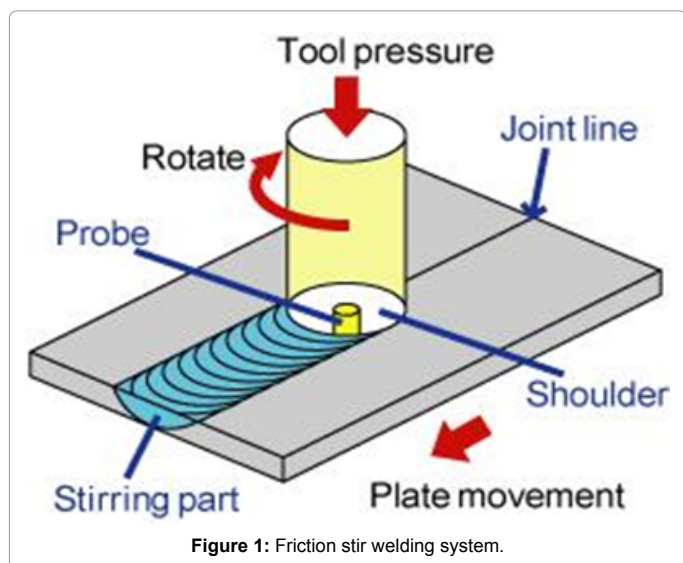

Figure 1: Friction stir welding system.

CTH hydro-code based on finite volume to model the flow of the material on the assumption that the material sticks to the tool surface [9]. Residual stress analysis was investigated using 3D thermal and thermo-mechanical numerical simulations [17]. This model used symmetry about the weld line, however this won't be accurate since friction stir welding is not symmetrical due the presence of advancing and retreating sides that are not identical.

The present work aims at development of a numerical and physical models to predict the process behavior in Friction Stir Welding. The numerical model is used for process design of friction stir welding operations using a non linear finite element techniques to characterize thermal and deformation behavior during friction stir welding high strength aluminum alloys. An empirical model is developed using design of experiments to relate the process parameters to the properties of the weld. Finally, case studies were conducted to validate the numerical model.

Numerical Modelling

Coupled temperature-displacement analysis

Coupled Temperature-Displacement analysis is used to model friction stir welding using ABAQUS-Explicit [18]. In this analysis, temperature and mechanical responses are determined simultaneously. Heat generated during friction stir welding is produced by friction between tool's shoulder and probe with sheet material and plastic deformation energy. Heat loss from sheet is due to convection from exterior surfaces of sheet and conduction from bottom surface of sheet to the backing plate.

Finite element method

Friction stir welding processes are inherently nonlinear because of the large strains, high temperature, and plastic behavior of the material in the welding zone. Complex nature of the interface friction conditions between the material and tooling surfaces adds to the difficulty of modeling the process. The standard "implicit" finite element formulation is a true quasi-static solution. However, in applications such as FSW, the standard method would yield very large linear matrix equation which must be solved for each load step [19]. The irregular nature of the interface friction will add to the complexity of the solution and make convergence extremely difficult and time consuming for each load step. The explicit method on the other hand [16] is basically a dynamic solution procedure through the application of explicit time integration to the discrete equation of motion. Total computation time in this method can be reduced by scaling up velocity and mass. Scaling velocity beyond certain limit might introduce non-realistic dynamic effects that can result in inaccuracy of the solution. Limiting punch speed in the simulation to less than 1% of the wave speed in the workpiece material would not significantly affect the solution accuracy [19]. In the present case of Aluminum Alloys with wave speeds of 5600 m/s, a welding speed up to 50 m/s will not affect the accuracy of the solution. Interface friction can be simulated in much simpler way than in the standard method. Furthermore, there is no convergence problems associated with the explicit approach. In the present work, the explicit method in ABAQUS is used to model the behavior of friction stir welding processes.

Three types or surfaces used in finite element analysis are Lagrangian, Eulerian and Sliding. Displacement in normal and tangential directions will follow the material in Lagrangian Surface. In Eulerian surface, the material is allowed to flow through the mesh. The mesh is fixed in all direction for eulerian surface. For sliding surface, mesh will follow the material in normal direction, while in tangential direction the mesh is fixed. Thus, top and bottom surfaces are modeled as sliding surface and other surfaces are modeled as Eulerian surface.

In Friction Stir Welding, there is considerable amount of material flow around the tool pin and contact forces. This will lead severe element distortion and ultimately lead to premature termination of the analysis. In order to overcome this mesh distortion during large plastic deformation, Arbitrary Lagrangian-Eulerian (ALE) technique has been used. Adaptive meshing with re-meshing has been employed to reduce large element distortion in modeling friction stir welding. Re-meshing improves the quality of the mesh as the analysis sweeps the mesh for every preset increment and the results are remapped to the improved mesh.

Governing Equations for Mechanical Analysis

ABAQUS/Explicit solves for a state of dynamic equilibrium at the start of current time increment t:

$$M^{NM} \ddot{u}^N \big|_t = \left(P^M - I^M \right)\big|_t \tag{1}$$

where M^{NM} is the mass matrix, u^N is the acceleration vector, P^M is the external force or applied load vector, and I^M is the internal force vector (the 'internal force' created by stresses in the elements). In the explicit procedure, a diagonal mass matrix is used for efficiency. Thus the nodal acceleration can be easily obtained:

$$\ddot{u}^N \big|_t = \left[M^{NM} \right]^{-1} \cdot \left(P^M - I^M \right)\big|_t \tag{2}$$

The central difference integration rule is used to update the velocities and displacements:

$$\dot{u}^N \bigg|_{t+\frac{\Delta t}{2}} = \dot{u}^N \bigg|_{t-\frac{\Delta t}{2}} + \left(\frac{\Delta t\big|_{t+\Delta t} + \Delta t\big|_t}{2} \right) \ddot{u}^N \big|_t$$

$$u^N \big|_{t+\Delta t} = u^N \big|_t + \Delta t\big|_{t+\Delta t} \, \dot{u}^N \bigg|_{t+\frac{\Delta t}{2}} \tag{3}$$

No iterations are required in the equation solver to update the accelerations, velocities, and displacements; so it is computationally economical for big model size like the cases addressed in this research. The stability of the solution depends on the time increment size, which is approximated as the smallest transit time of a dilatational wave across any of the element in the mesh.

$$\Delta t \approx \frac{L_{\min}}{c_d} \tag{4}$$

In which $Lmin$ is the smallest element dimension in the mesh and cd is the dilatational wave speed.

Governing Equations for Thermal Analysis

In ABAQUS/Explicit, the heat transfer equations are integrated using the explicit forward-difference time integration rule.

$$\theta^N_{(i+1)} = \theta^N_{(i)} + \Delta t_{(i+1)} \dot{\theta}^N_{(i)} \tag{5}$$

where θ^N is the temperature at node N and the subscript i refers to the increment number in an explicit dynamic step. The forward-difference integration is explicit in the sense that no equations need to be solved when a lumped capacitance matrix is used. The current temperatures are obtained using known values of $\dot{\theta}^N_{(i)}$ from the previous increment.

In order to simulate friction stir welding process accurately, heat generation by both friction and plastic deformation are modeled rather

than adding heat flux to the tool.

$$qA = f\eta Pfr \text{ and } qB = (1-f)\eta Pfr \qquad (6)$$

Where qA is the heat flux into the sheet and qB is the heat flux into the tool.

f is the percent of heat flux that flows into the sheet (0.0 to 1.0)

η is the factor of converting mechanical to thermal energy Pfr is the frictional energy dissipation.

Plastic straining gives rise to a heat flux per unit volume.

$$r^{pl} = \eta\sigma : \dot{\varepsilon}^{pl} \qquad (7)$$

Where r^{pl} is the heat flux that is added into the thermal energy balance, η is the factor for percent of heat converted, σ is the flow stress of the material, and $\dot{\varepsilon}^{pl}$ is the rate of plastic straining.

The Johnson-Cook Strain Rate dependent flow stress is used as the constitutive equation to describe the flow stress behavior of the material during processing.

$$\bar{\sigma} = \left[A + B\left(\bar{\varepsilon}^{pl}\right)^n \right]\left[1 + C\ln\left(\frac{\bar{\varepsilon}^{pl}}{\dot{\varepsilon}_0}\right)\right]\left(1 - \hat{\theta}^m\right) \qquad (8)$$

Where $\bar{\sigma}$ is the effective flow stress, $\bar{\varepsilon}^{pl}$ is the effective plastic strain is $\dot{\varepsilon}_0$ the normalizing strain rate, A, B, C, n, m are the material constants (Table 1).

$$\hat{\theta} = \begin{cases} 0 & for & \theta \le \theta_{transition} \\ (\theta - \theta_{trension})/(\theta_{melt} - \theta_{transition}) & for & \theta_{transition} \le \theta \le \theta_{melt} \\ 1 & for & \theta \ge \theta_{melt} \end{cases} \qquad (9)$$

Where θ is the current temperature, $\theta melt$ is the melting temperature and $\theta transition$ is the transition temperature below which there is no temperature dependence on flow stress.

Heat loss due to conduction and convection is considered in this research. Heat loss is modeled from bottom of the plate to the backing plate. Conductive heat loss is given by,

$$q = k(\theta_A - \theta_B) \qquad (10)$$

Where q is the heat flux, K is the conductivity, θ^A and θ^B are the temperatures at point A and B on the surface.

Heat loss due to convection is considered from all exterior surfaces of the sheet. Heat flux due to convection is given by:

$$q - h(\theta - \theta^0) \qquad (11)$$

Where q is the heat flux, h is the film co-efficient, θ is the temperature at the surface θ^0 is the sink temperature.

The developed model deals with characterization of the responses of the material to the mechanical and thermal loading environment generated by friction stir welding. This model provides guidance for selecting the appropriate process conditions that result in desirable properties of the joint.

Experimental Investigation

Experimental setup

Friction Stir Welds were produced using an in-house built FSW system based on an available milling machine. Two Al 2024-T3 sheets of dimensions 50 mm × 50 mm × 2 mm were rigidly clamped on a titanium backing plate which is fixed to a steel base. The two sheets are

then butt welded using the rotating FSW tool with a shoulder diameter of 18 mm. The tool's probe has diameter of 6 mm and a height of 1.9 mm. The base metal properties are given in Table 1.

Statistical design of experiments

A set of experiments was designed using the response surface methodology (RSM) [20]. RSM methodology is a collection of statistical and mathematical techniques effective for modelling and optimization of manufacturing process designs. Central composite designs in RSM, are vastly used for fitting second-order response surface because of both their statistical properties and the practical attraction of their expanded coverage around a centre point [20]. In the present research, RSM is used to investigate the effects of the control process parameters that include rotational speed and feed rate (welding speed) on the important quality characteristics of the joint. The experimental matrix used in the present investigation is presented in Table 2.

In the present study, a second-order response surface model (equation 12) is used to formulate a least square relationship between the input parameters and the output response measures.

$$Z = \beta_0 + \beta_1 X + \beta_2 Y + \beta_{11} X_2 + \beta_{22} Y_2 + \beta_{12} XY \qquad (12)$$

Where Z are the observed responses (formability of the joint measured by reduction of area % at fracture), as a function of the main influences of factors X (rotational speed, RPM) and Y (feed rate, IPM), their interaction (XY), and their quadratic components (X^2, Y^2). β_0, β_1,…etc. are estimated regression coefficients.

Evaluation of Properties of FSW joints

Mechanical properties of the friction stir welded joints were evaluated using standard tensile test procedures. The gage dimensions of the specimens were 25.4mm (1") long and 19mm (3/4") wide and with the weld zone running across the gage length.

The test speed was kept constant at 1 cm /min for the duration of the test.

Results and Discussions

Prediction of process behaviour using numerical models

In order to evaluate the effectiveness of the developed numerical model, two case studies for friction stir welding of Al 2024-T3 were conducted. One case was chosen to represent sound joint and another one represents the condition of bad joint. The process parameters for both cases were selected based on preliminary experimental evaluation conducted by the authors on the investigated material. Table 3 presents

Material Properties	Al 2024-T3
Density (Kg/cc)	2780
Modulus of Elasticity (GPA)	73
Poisson's Ratio	0.33
Ultimate Tensile Strength (MPa)	483
Yield Stress, A (MPa)	369
Strain Factor, B (MPa)	684
Strain Exponent, n	0.73
Temperature Exponent, m	1.7
Strain Rate Factor, C	0.0083
θmelt (°C)	502
θtransition (°C)	25
Thermal Conductivity (W/m-K)	121
Specific Heat Capacity (J/Kg °C)	875

Table 1: Material properties of Al 2024-T3.

Exp. #	1	2	3	4	5	6	7	8	9(c)	10(c)	11(c)	12(c)	13(c)
Rotational Speed(RPM)	840	840	1300	1300	675	1300	1045	1045	1045	1045	1045	1045	1045
Feed Rate(IPM)	4.625	7.625	4.625	7.625	5.75	5.75	3.625	7.625	5.75	5.75	5.75	5.75	5.75

Table 2: Experimental matrix using RSM.

Process Parameters	Case 1	Case 2
Welding Velocity (mm/sec)	2.43	2.43
Rotational Velocity of Tool (rpm)	1045	445
Co-efficient of Friction	0.3	0.3
Effective Plunge Depth (mm)	2	1.9

Table 3: Process parameters for case studies.

the levels of the control parameters used for good weld (Case 1), and bad weld (Case 2). Other friction stir welding process parameters were kept constant. They include: Plunge time (5 seconds), Dwell time (15 seconds), and Pull time (5 seconds).

Numerical modeling results using the conditions listed for Case 1 are displayed in Figures 2-5. Figure 2 displays temperature distribution fields along the weld line at the end of welding process. Temperature distribution across the width of entire blank is show in Figure 3. The temperature in area adjacent to the tool is the highest (538°C). The evolved temperature field is extended to cover the entire blank because of the active heat transfer by convection due to the flow of heated material and conduction to the neighboring zones. The lowest temperature in the field during FSW is 45°C. The close spacing between isotherms in the neighborhood of tool/work-piece interface is anindication that heat is generated at that spot and then dissipated by convection and conduction to other zones in the panel. Figure 4 displays the progress of the heat source as the tool travels along the weld line. Equivalent plastic strain along the joint-line is shown in Figure 5. Plastic strains represent degree of deformation as result of the stirring action during the process. The extent of the zone with high level of plastic strain (highly deformed region) along the weld line is an indication of the size of the weld nugget and the adjacent thermo-mechanical affected zone (TMAZ). One can conclude that simulation results presented in Figure 2 through Figure 5 can be used to evaluate alternative process designs in order to explore the optimum one.

In the second case study, conditions not favorable for a successful weld are investigated. All process parameters are kept the same except using reduced rotational velocity and smaller plunge depth. These conditions do not allow the establishment of sticking friction between the tool shoulder and the surface of the base metal. Hence no sufficient heat is generated and the hot flow of material needed to fill the joint gab is ceased. A groove is generated along the joint line as a result of removing instead of depositing material behind the FSW tool. This is evident in Figure 6. The evolved temperature fields for this case are also displayed in Figure 6. Maximum temperature along the joint never exceeded 110°C which is not sufficient to establish softening by dynamic re-crystallization in the material Figure 7.

Experimental characterization of FSW process behaviour

Case studies simulated using the numerical models in section 4.1 were verified experimentally through running FSW of Al 2024 T3 blanks according to the process conditions described in Table 3. Figure 8 shows an established FSW joint using parameters of case 1. Conducting FSW according to conditions described in case 2 resulted in poor joint. Because of insufficient temperature rise along the joint, FSW tool created a groove instead of depositing material along the weld
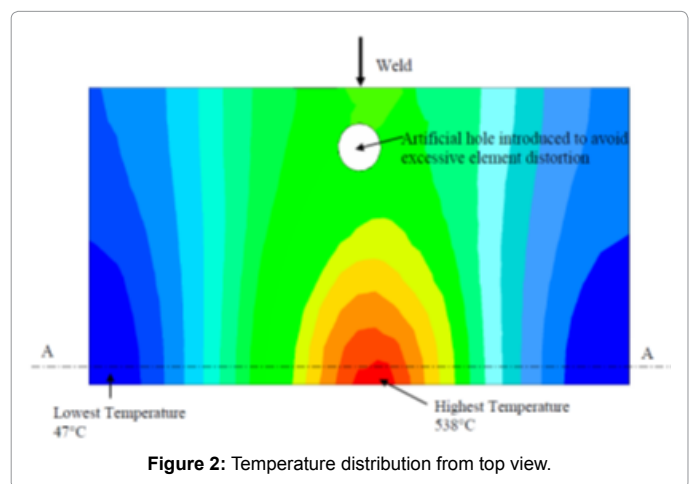

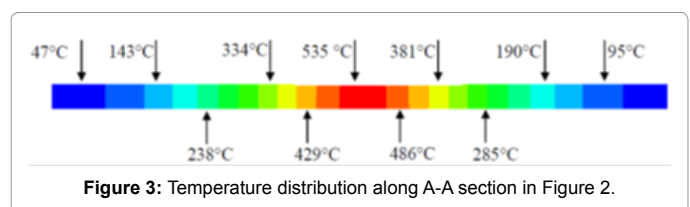**Figure 2:** Temperature distribution from top view.

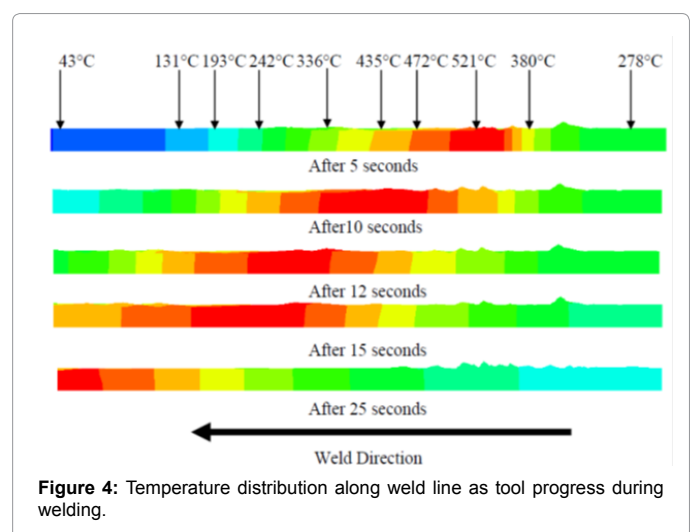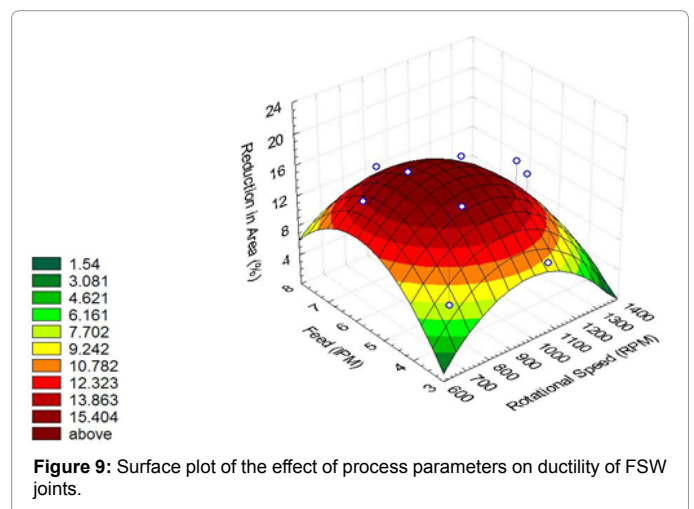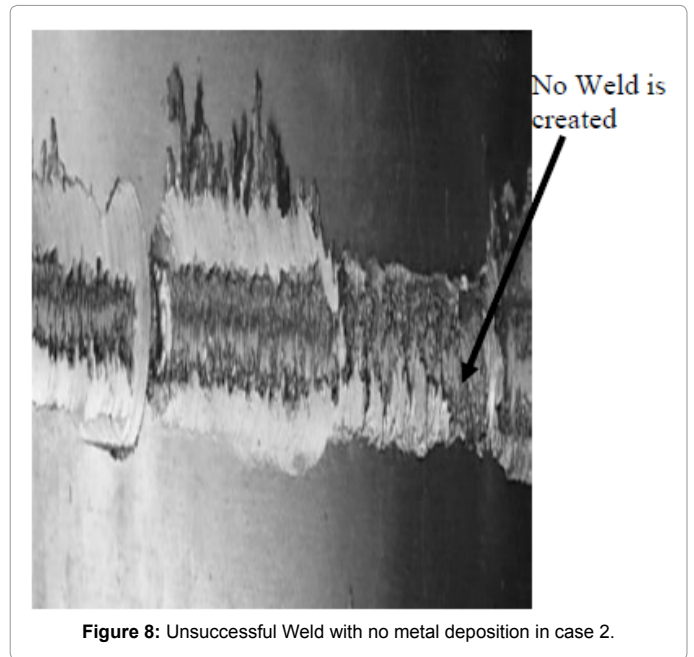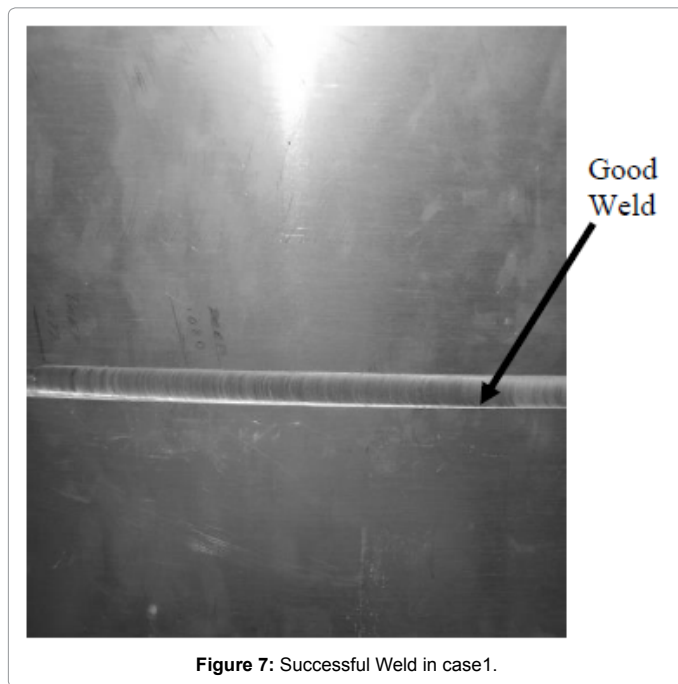**Figure 3:** Temperature distribution along A-A section in Figure 2.

Figure 4: Temperature distribution along weld line as tool progress during welding.

line see Figure 9.

Figure 5: Equivalent Plastic Strain.

Figure 6: Insufficient temperature distribution.

Figure 8: Unsuccessful Weld with no metal deposition in case 2.

Figure 7: Successful Weld in case1.

Figure 9: Surface plot of the effect of process parameters on ductility of FSW joints.
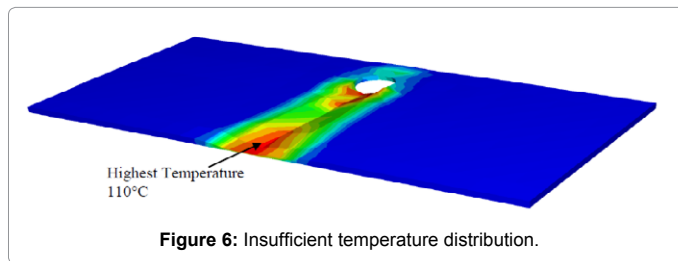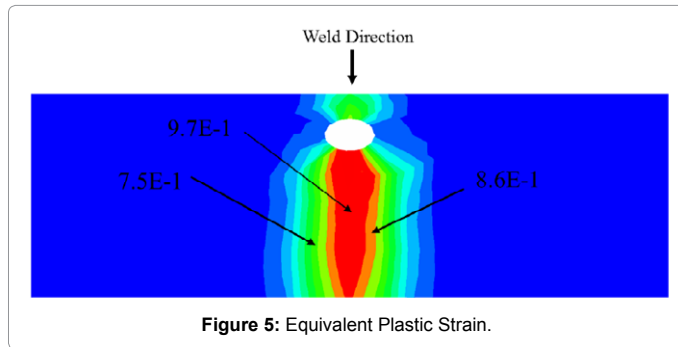
These results compare very well with the prediction of the numerical model. Temperature indicating paints have been used check the establishment of particular temperature field during FSW process. The measured temperatures were very close to the predicted ones using the developed numerical models.

Friction stir welding process-induced properties

The design of experiments defined in section 3.2, were used to collect data on the effect of FSW process parameters on evolved strength and ductility of the welded joints. Data in Table 4 represents strength and ductility measures of joints established using different combinations of rotational speed and feed rate (welding velocity). From the results shown in Table 4, condition in experiment #5 (rotational speed of 1045rpm and welding speed of 2.43 mm/sec) created the weld with the most desirable properties. It has the best combination of strength and ductility (high toughness). All the results were also fitted to three dimensional surfaces relating the effect of the independent variables (rotational speed and feed) on one of the quality characteristics of the process. A typical presentation of response surface for ductility is displayed in Figure 10. In this plot, ductility of the joint as measured by the reduction of area% was selected as the major response. The process contour map for joint ductility extracted from the surface plot is shown in Figure 10. Both figures indicate that rotational speed in the range of 800 to 1100 rpm and welding speed of 4.5-6.5 inch/min (114-165 mm/min) would yield optimum joint ductility. Similar surface plots and contour maps for the ultimate strength and yield strength were also generated from the results.

Conclusions

1. A numerical model uses a non-linear finite element method is developed to characterize thermal and deformation behavior along the

#	Rot. Vel.(RPM)	Weld Vel.		% Elong	% Red.In Area	YS		UTS	
		(mm/sec)	(IPM)			(MPa)	(PSI)	(MPa)	(PSI)
1	1300	0.9	2.125	12.37	14.58	211.52	30678.44	324.28	47032.92
2	1300	1.53	3.625	16	12.13	319.36	46319.34	437.66	63477.33
3	1300	2.43	5.75	10.67	5.95	313.17	45421.55	407.01	59031.92
4	1300	3.23	7.625	6.49	9.23	301.38	43711.55	429.48	62290.92
5	1045	2.43	5.75	18.18	17.08	309.75	44925.52	449.86	65246.79
6	1045	1.53	3.625	11.4	7.09	330.66	47958.27	445.23	64575.27
7	1045	3.23	7.625	8.49	8.85	314.57	45624.6	424.62	61586.04
8	840	1.96	4.625	12.73	11.17	303.69	44046.59	418.08	60637.49
9	840	2.43	5.75	11.18	10.03	310.56	45043	424.73	61601.99

Table 4: Mechanical properties from design of experiments.
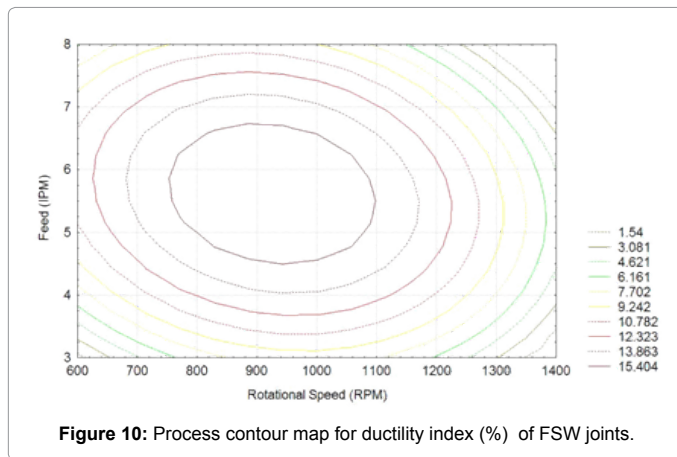

Figure 10: Process contour map for ductility index (%) of FSW joints.

weld line during friction stir welding process.

2. Coupled Temperature-Displacement analysis is used in the FEM model in order to allow for simultaneous determination of temperature, displacement, and mechanical responses.

3. Experimental verification of the proposed numerical models for friction stir welding was conducted using two case studies. The experimental observations confirm the predictions of the models.

4. The results obtained using the design of experiments and surface response methodology offer insights into the effects of the major process parameters in establishing successful FSW joints with optimum strength and ductility that satisfy further processing requirements and product service conditions.

5. The results generated from the present investigation were used for constructing process maps for FSW of Al 2024-T3. These maps are effective tools that can be used by industry as road maps in selecting process designs that satisfy both quality requirements and productivity constraints.

Acknowledgements

References

1. Thomas WM, Nicholas ED, Need ham JC, Murch MG, Templesmith P, et al. (1991) Friction Stir Welding.

2. Mishra RS (2003) Friction stir processing technologies. Advan Mater & Processes 43-46.

3. Mishra RS, Ma ZY (2005) Friction stir welding and processing. Mater Sci Eng 50: 1-78.

4. Nandan R, DebRoy T, Bhadeshia HKDH (2008) Recent advances in friction-stir welding - Process weldment structure and properties. Progr in Mater Sci 53: 980-1023.

5. Tang W, Guo X, McClure JC, Murr LE, Nunes A (1998) Heat input and temperature distribution in friction stir welding. J Mater Processing Manufacturing Sci 7: 163-172.

6. Heurtier P, Jones MJ, Desrayaud C, Driver JH, Montheillet F, et al. (2006) Mechanical and thermal modeling of friction stir welding. J Mater Processing Technol 171: 348-357.

7. Palm F, Hennebohle U, Erofeev V, Earpuchin E, Zaitzev O (2004) Improved verification of FSW-process modeling relating to the origin of material plasticity. P Fifth Int Symposium of Friction Stir Welding TWI Ltd Metz France.

8. Ulysee P (2002) Three dimensional modeling of the friction stir welding process. Int J Mach. Tools Manufacture 42: 1549-1557.

9. Askari A, Silling S, London B, Mahoney M (2001) Modeling and analysis of friction stir welding processing. In: Jata KV (ed.) Friction Stir Welding and Processing TMS Warrendale, PA : 43-54.

10. Padmanaban R, Ratna V, Balusamy V (2014) Numerical simulation of temperature distribution and material flow during friction stir welding of dissimilar aluminum alloys. P Eng 97: 854-863.

11. Kesharwania RK, Pandab SK, Palc SK (2014) Multi Objective Optimization of Friction Stir Welding Parameters for Joining of Two Dissimilar Thin Aluminum Sheets. P Mater Sci 6: 178-187.

12. Kimapong K, Wanabe T (2004) Friction stir welding of aluminum alloy to steel. Welding J 83: 277-282.

13. Hunt F, Badarinarayan H, Okamoto K (2006) Design of experiments for friction stir stitch welding of aluminum alloy 6022-T4. SAE Int: 173-178.

14. Chao YJ, Qi X (1998) Heat Transfer and Thermo-Mechanical analysis of friction stir joining of AA 6061-T6 plates. J Mater Processing Manufacture Sci: 215-233.

15. Frigaard F, Grong F, Midling OT (2001) A process model for friction stir welding of age hardening aluminum alloys. Metallurgical Mater Transactions A 32: 1189-1200.

16. Zahedul M, Khandkar H, Khan J (2001) Thermal modeling of overlap friction stir welding for Al alloys. J MaterProcessing Manufacture Sci 10: 91-106.

17. Zhu XK, Chao YJ (2004) Numerical simulation of transient temperature and residual stresses in friction stir welding of 304L stainless steel. J Mater Processing Technol 146: 263-272.

18. ABAQUS version 6.9 Internet Manual.

19. El-Gizawy AS, Chitti Babu S, Yeh T (2004) An integrated virtual model for characterization and management of process-induced damage in sheet forming processes. P 4th CIRP Int. Seminar on Intelligent Computation in Mfg Eng Naples Italy: 321-326.

20. Mayers RH, Montgomery DC, Anderson Kook CM (2009) Response surface methodology-process and product optimization using design of experiments. 3rd edn John Wiley & Sons Inc Hoboken New Jersey.